JOURNAL OF
EMERGING INVESTIGATORS

Article

Influence of polygon side number on laminar vortex shedding frequency and variability

Yilin Liuhan[1], Toby Bryce-Smith[2]
[1] Eton College, Windsor, Berkshire, United Kingdom
[2] Imperial College London, London, United Kingdom

SUMMARY

The geometry of polygonal bodies influences unsteady aerodynamic forces exerted from vortex shedding. Prior research has shown sensitivity of a polygon's shedding frequency to the number of sides and rotational position; however, only a narrow region of Reynolds numbers have been tested, meaning that shedding behavior within different fluidic regimes are yet to be explored. We investigated these shedding characteristics at a Reynolds number of 200, focusing on frequency variation and separation behavior. We hypothesized that as the number of sides of the polygon increases, variation in the shedding frequency would decrease due to a reduced variation in the separation point over the polygon. We created a computational fluid dynamics solver to test nine test cases with varying side numbers and angular positions to test this hypothesis. Our results support this hypothesis: we observed an 83% decrease in the range of separation point and a 90% decrease in the standard deviation of shedding frequency comparing octagonal to square polygons. Furthermore, we suggest a new definition for polygonal rotational position that differs from convention, instead defined by the top facing geometry based on the grouping of maximum and minimum shedding frequencies being reversed for the hexagonal case compared to the square and octagonal cases. Results from this work show that designers must consider the variation of vortex shedding frequency for low-sided polygons to reduce the range of frequencies that structures must tolerate, for example, in oil pipelines subjected to ocean currents and large skyscrapers immersed in the wind.

INTRODUCTION

Polygonal geometries are highly common in both nature and the engineered world, therefore, the fluid flowfield over them is of great interest. Polygons have a low aspect ratio which gives the fluid flowfield a different set of physical phenomena compared to streamlined geometries (e.g., aircraft wings). As a fluid flows over a polygonal body, it leaves behind a wake with different characteristics depending on the properties and state of the flow (1). Within this wake, a key fluidic structure that forms are discrete vortices which are defined as regions of high circulation of fluid, such as hurricanes. Under certain flow conditions, an asymmetric pattern of vortices (rotating packets of fluid) forms in its wake, known as a 'von Kármán vortex street' (2). These patterns are periodic, meaning that they have a clear 'shedding frequency' associated with them. Since antiquity, humans have observed periodic vortex shedding over polygonal (or pseudo-polygonal) bodies – either directly through water trails and cloud formations or indirectly via acoustic resonance caused by vortex shedding, referred to as aeolian tones. In 1912, von Kármán provided a theoretical explanation for the regular vortex pattern caused by vortex shedding. Periodic vortex shedding is common in nature. For example, winds flowing past a mountain, a structure with a pseudo-polygonal cross-section, can cause vortices to be visible within the clouds (3). Similarly, fish tune their body wavelength and tail motion to the shedding frequency to extract energy from the vortices and reduce their own propulsive effort (4). As such, the physics of periodic vortex shedding remains a key area of academic interest.

The flowfield around a polygonal body is characterized by flow separation, where the fluid effectively leaves the surface of the body. There is a high force associated with this, known as a drag force. Additionally, a vortex is shed and the swirling air inside it lowers the static pressure within the vortex, which can be observed in the low atmospheric pressures that surround hurricanes (5). As the pressure near a vortex is lower, a force is felt by the body. As the shedding alternates sides, an oscillatory force is applied to the body. These oscillatory loads have important engineering consequences. A wide range of engineered structures have polygonal geometries and interact with fluids – for example, skyscrapers and wind turbine towers in atmospheric flows, and oil pipelines exposed to ocean currents, which lead to material fatigue or failure over time. If the shedding frequency approaches or equals the natural vibration frequency of the structure, resonance can occur, building energy over time causing vortex-induced vibrations that can destroy a structure entirely, most famously in the 1940 Tacoma Narrows bridge collapse (6). Therefore, unsteady forces from fluid-structure interaction are an important consideration for safety in engineering design.

Shedding frequency is a key factor in characterizing vortex shedding. Multiple factors influence a flow's shedding frequency over a polygonal body, therefore, yielding wide academic interest. The shedding frequency of a polygonal cylinder has been shown to significantly vary with side number, N. For polygons with $N \leq 8$, the point of separation largely occurs at sharp corners, which is shown to affect shedding frequency (7). Additionally, the angular position of the polygon with respect to the fluid flow direction has been experimentally shown to affect shedding frequency (7). Crucially, these results occur in a specific fluidic region characterized by the dimensionless ratio of inertial forces to viscous forces, the Reynolds number, $Re = \rho vL/\mu$ (where ρ is the fluid density, v is flow velocity, l is characteristic length, and μ is the dynamic

https://doi.org/10.59720/25-121

viscosity of the fluid) with a reported Reynolds number region for these shedding characteristics between 1,000 and 4,000 (7). Other parameters that affect shedding frequency include surface roughness and porosity (8). As a crucial dependence of polygonal shedding characteristics occurs within the region 1,000 < *Re* < 4,000, has been widely reported, further studies are required to further elucidate shedding behavior in different Reynolds number regions

We investigated how the number of sides and angular orientation of a polygon affect its vortex shedding behavior. By studying shedding characteristics at a Reynolds number of 200, we tested the applicability of trends reported at higher Reynolds numbers and explored whether different flow features that are unique to low-Reynolds-number conditions emerged. We hypothesized that, as the number of sides of the polygon increases, a reduced variation in the shedding frequency will be observed due to a reduced variation in the separation point over the polygon. We created a computational fluid dynamics (CFD) solver to test the shedding characteristics of polygons with four, six, and eight sides, in three angular positions respectively at a Reynolds number of 200 that to our best knowledge has not been reported before. Our results support this hypothesis, showing a consistently reduced variation of shedding frequency across the test cases. Furthermore, the shedding behavior of the test cases showed convergence towards that expected from a circular cylinder. Our results add further computational data at a new set of flowfield properties and will aid engineers towards more informed designs for bluff-bodied structures immersed in fluid flow.

RESULTS

In order to quantify the variation in shedding frequency between each test case, we ran the CFD solver over a number of vortex shedding cycles. We define the CFD domain (the region of fluid that is simulated) as a 2D region with streamwise lengths of 7L and 20L, upstream and downstream, respectively, where L denotes the characteristic length of the polygon within the domain **(Figure 1)**. We then enforce boundary conditions at the walls along with general solver settings as outlined in the Material & Methods section.

At the point of vortex shedding, we observed significant velocity fluctuations associated with the vortices. We assessed

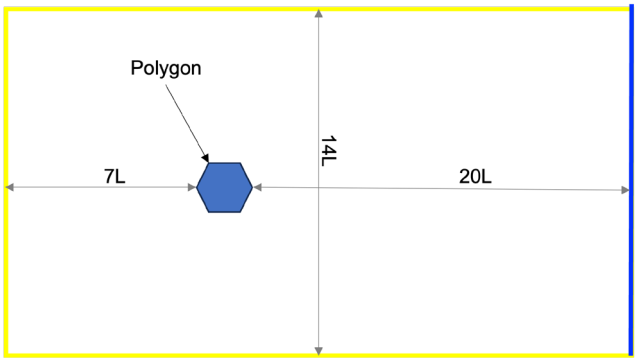

Figure 1: Computational Fluid Dynamics study setup diagram. Diagram of the CFD domain. Blue walls represent velocity outlets and yellow walls represent velocity inlets; the polygon is shown in blue. L represents its characteristic length.

the velocity time series at these locations, performing a fast Fourier transform, to capture the shedding frequency. Finally, we convert this frequency into the dimensionless Strouhal number, $St = fL/U$, (where f is the frequency of vortex shedding, and U is the flow velocity), to enable direct comparison to polygons from other studies and in the wider engineering world. Herein, we report the collected shedding frequency as a Strouhal number in line with engineering standards (7,8).

The variation of the Strouhal number between the angular rotations of the polygon decreased as the number of sides increased (**Figure 2**). Cases are defined herein as two characters (e.g., '4C'), the first being their side number and second indicating the angular rotation defined by the leading geometry in the streamwise direction: C and F representing a corner or face, and H representing a half step between the two. This follows convention from other polygonal studies (7). The most notable decrease in variability occurs between the hexagonal and octagonal cases, as shown by the decrease in the order of magnitude of standard deviation (**Table 1**). The variation of cases within the square cases was also non-linear, as 4C and 4F have similar values of St, but the large standard deviation is caused by the 4H case. No distinct pattern emerged for which angular rotation produced the maximum or minimum values for each polygon; for example, 4F and 8F showed the smallest Strouhal number for the square and octagon cases, but 6F had the largest Strouhal number for the hexagon case (**Figure 2**).

We identified the fluid's time-averaged separation point for each case from the skin friction coefficient (**Figure 3**). The separation point is defined in this study as the location where the skin friction coefficient is zero, even if downstream the flow 'reattaches' leading to a non-zero value (**Figure 4**). As the number of sides increased, the variation in separation point across the three angular positions decreased **(Table 1)**. We observed that the square cases had the largest variation in separation point, with a range of 135 degrees, notably with the separation point shifting all the way to the trailing edge for case 4C. We saw a 44.4% decrease in variation of range for the hexagonal test cases, and a further 70% reduction for the octagonal cases. While the percentage drop from hexagon to octagon was more dramatic than the drop from square to hexagon, the actual decrease in range was 7.5 degrees greater between the square and the hexagon. We observed that the forwardmost and aftmost separation points were the F and C cases for the square and octagon, but we observed a different result from the hexagon with H and C instead (**Figure 2**).

The drag coefficient, $2F_d/(\rho A v^2)$, F_d is the drag force and A is the reference area, representing the dimensionless loading on the shape; therefore, a larger drag coefficient leads to larger forces on the structure. The mean value of the drag coefficient decreased as the number of sides increased **(Table 1)**. The average drag coefficient in the square, hexagon, and octagon cases were 2.587, 1.841, and 1.563 respectively. The most prominent decrease in the magnitude of variation between the angular positions was from square to hexagon. The most prominent decrease in the standard deviation between the angular positions was 81% for the hexagonal cases to the octagonal cases. The lowest drag for each shape was seen on 4F, 6C, and 8F, with the highest drag on 4C, 6F, and 8C. A

https://doi.org/10.59720/25-121

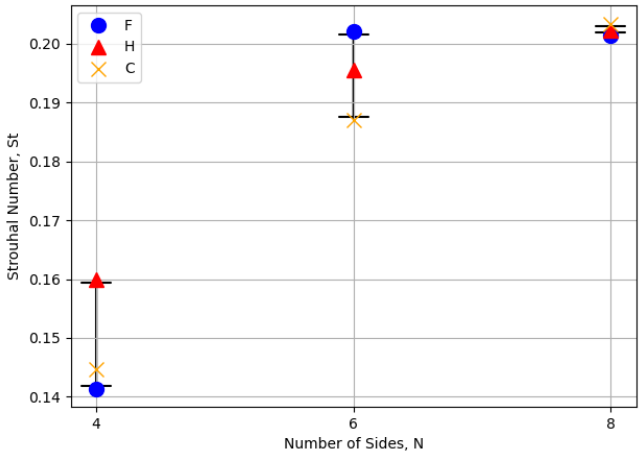

Figure 2: Comparison of the variation in Strouhal number as number of sides of the polygon increases. A graph showing how angular rotation affects Strouhal number and how as the number of sides increased, the variation decreased. The black bar represents the variation of Strouhal number for each polygon. The three markers represent the rotational positions of the polygon: F (face-aligned), C (corner-aligned), and H (half step), with assigned markers of blue circle, yellow cross, and red triangle respectively.

notable alternating trend exists for these three cases.

To visualize the polygon's shedding, we plotted the instantaneous vorticity, a scalar quantity for a two-dimensional (2D) flow representing local rotation of fluid where $\omega=\partial v/\partial x - \partial u/\partial y$, at a consistent point in the periodic shedding cycle, as this shows the outer regions of the polygon's wake. We observed a visual reduction in variation of the shed vortex paths resulting from angular rotation as the number of sides increases (**Figure 5**). This is especially apparent in the area behind the polygon, with the square case showcasing three different patterns of vorticity, to the octagon showing a general consistent pattern as the polygon is rotated. The forces that the fluid imparts onto the cylinder is directly related to the size of the wake.

DISCUSSION

For all metrics studied, increasing the number of sides reduced variation in shedding frequency due to angular position changes. Notably, the separation point for all test cases was at a corner, in line with prior studies (7). As the number of sides of the polygon increased, we rotated the polygon less to achieve each test case position. Since our separation point was directly controlled by each test case's corners, we saw reduced variation in the shedding frequencies as we increased the number of sides of the polygon, owing to the reduced rotation in the polygon (**Figure 2**). We observed this in both the change of standard deviation between the cases, but also visually in the instantaneous vorticity plot showing the wake shape between each case (**Figure 5**). Furthermore, for each polygon, we observed the largest drops in variation for both the shedding frequency and the separation point between the hexagon and the octagon. We therefore conclude that as we increase the number of sides, there is a reduced variation in fluid separation point over the polygon, which reduces the variation of shedding frequency, in line with our initial hypothesis.

We observed that the 4F and 8F cases yielded the lowest shedding frequency for their respective shapes while 6F yielded the highest (**Figure 2**). As noted previously, the separation points are controlled by each shape's corners (**Figure 3**). Despite these cases being defined based on the geometry of the leading face being perpendicular to the flow, the variation of side number leads to the profile of each shape at 90 degrees being drastically different; 4F and 8F have flat sides at 90 degrees, while 6F has a corner at 90 degrees (**Figure 3**). As a shape's separation point is typically near this location, we do not see consistent behavior. This trend is further highlighted in the drag coefficient, where the 'C' and 'F' cases alternated between maximum and minimum drag. These results suggest that the nomenclature used in this study, which is also widely used within polygonal cylinder studies, to categorize test cases by rotation angle, should be redefined (7). We find from this study that the more appropriate geometric definition is for the orientation of faces near the separation point at 90 degrees, rather than the front-facing edge.

There are some limitations of our study that stem from our model and our underlying assumptions. We used a 2D CFD model, which failed to capture any out-of-plane motions and could under/over-predict certain flow quantities. Real-life structures are all three-dimensional (3D), so a 2D study can only provide insights with assumptions, such as the absence of fluid flow in the out-of-plane dimension. The geometry of the polygons used also assumes a perfectly smooth surface and sharp corners, which would not be the case on engineered designs. Geometrical variations to the polygon, such as barnacles on oil pipelines or erosion on aerofoils have been shown to alter the flowfield around a geometry (9,10). Furthermore, these results are only valid at a Reynolds number of 200, and no effects of changing the Reynolds number have been tested in this study owing to time limitations. Finally, only three test cases can be used within this study for assessing trends due to limitations in the computational solver. Expanding the computational solver to capture higher side number geometries would enable these trends to be extended beyond N = 8.

In this computational study, we used a 2D CFD solver to test the effects of rotation and side number to test that variation

Test Case	4C	4F	4H	6C	6F	6H	8C	8F	8H
Separation Point (°)	45	158	180	60	90	135	90	67.5	78.8
Standard Deviation	72.3			37.7			11.3		
Average Value	127.7			95.0			78.8		
Strouhal number	0.145	0.141	0.160	0.187	0.202	0.196	0.203	0.202	0.202
Standard Deviation	0.00984			0.00752			0.000991		
Average Value	0.149			0.195			0.202		
Drag Coefficient	3.29	1.73	2.74	1.59	2.09	1.85	1.61	1.52	1.56
Standard Deviation	0.790			0.248			0.0473		
Average Value	2.59			1.84			1.56		

Table 1: Table of separation point and Strouhal number variation. A table comparing the separation point in degrees relative to the flow field and the variation in separation point and Strouhal number as the number of sides increases.

https://doi.org/10.59720/25-121

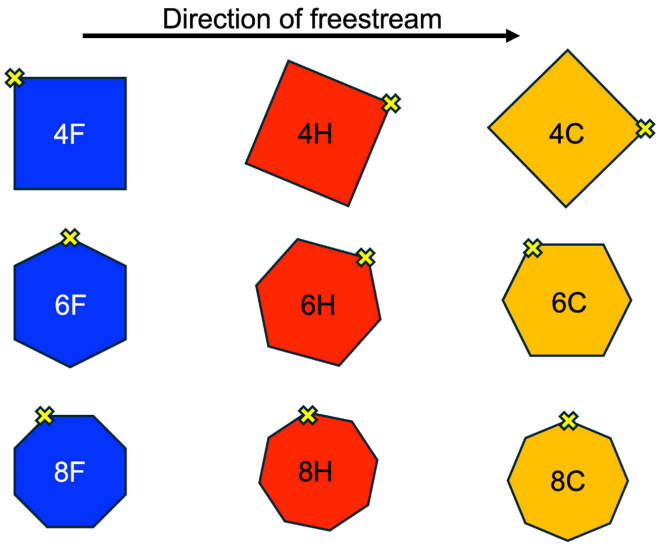

Figure 3: The nine test cases with their separation points. Each separation point (cross) was found by plotting the wall shear stress against the positional axis and the point where shear stress is zero. Freestream velocity is noted with the arrow at the top.

in vortex shedding behavior from rotating a polygonal cylinder will reduce as the side number increases. Our findings show that the angular position of a bluff polygonal body significantly affects the unsteady flowfield around it at a new Reynolds number range. Our results further suggest a redefinition of angular rotation should be used within polygonal shedding studies focusing on the geometry near the separation point rather than directly facing the flow.

Based on these results, an aerodynamicist should test designs at multiple test points, especially where a design has large rotations required for rotational symmetry such as seen in our square and hexagonal cases, to obtain a range of shedding frequencies to ensure no natural harmonics are within them. Engineers can look at trends from this data which can help tune designs to a more suitable shedding frequency, improving structural safety margins. Our results showed that the separation point is controlled by the corners of the polygon; therefore, further work could computationally investigate passive or active flow control devices to mimic polygonal cross-sections as done in this study. Results from this study could then help engineers tune a structure's periodic loading to different values without a polygonal shape being fixed in the design.

MATERIALS AND METHODS

CFD solver

To test our hypothesis, a laminar flowfield was simulated using a computational fluid dynamics (CFD) solver (**Figure 1**). To ensure that our results would be transferable to differently scaled flowfields, analyses were performed using the dimensionless Reynolds number, $Re=(\rho vL)/\mu$, where ρ is the fluid density, v is the fluid velocity, L is the polygon's characteristic length, and μ is the fluid's dynamic viscosity. The flowfield was tuned to a Reynolds number of 200 in order to test at a Reynolds number that, to our knowledge, has not been tested before in literature. Furthermore, at this Reynolds number, we could use a laminar CFD solver which made computations cheaper and less time-consuming to run on a personal computer.

A 2D CFD solver was created using the commercial CFD software, Fluent 2024 R2 to test the hypothesis (11). To match the target Reynolds number of 200, standard atmospheric conditions were used, using a dynamic viscosity of 1.789×10^{-5} Pa·s and atmospheric density of 1.225 kg/m³ (12). Then, freestream velocity was set at 0.292 m/s to fix the Reynolds number at 200.

Standard good CFD practice were followed to set up the domain dimensions (13). The rectangular domain had velocity inlets on the upstream and side walls (14 characteristic lengths tall), and a velocity outlet 20 characteristic lengths downstream (**Figure 1**). The downstream section of the domain was set to 20 characteristic lengths to allow for the capture of the wake.

To discretize the domain, a structured mesh was used to improve the solver accuracy. This was possible as the polygon tested fit well with the rectangular nature of the structured mesh. The area around the polygon had a finer, higher-density cell mesh to reduce discretization error near separation points. An inflation layer was then used so that the areas further away from the polygon had a larger cell size to reduce the overall cell count to decrease computational time whilst preserving the accuracy of the data. The overall cell count averaged 195,000. A mesh convergence study was performed to ensure discretization error with the global settings was minimized.

The solver then ran for each timestep until convergence was reached, defined as when all residuals were below 10^{-8} at the end of each iteration. No notable convergence issues were noted throughout the experiment. Each timestep was fixed at 0.5 ms to ensure shedding behavior was captured in

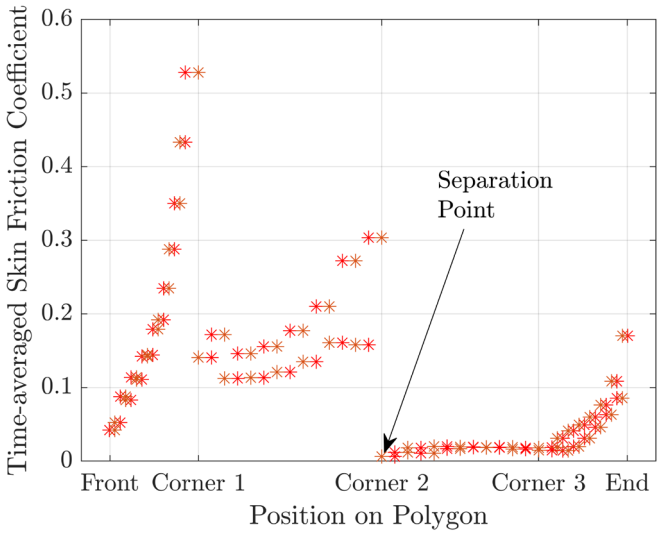

Figure 4: Friction graph to the separation point. A representation of the process taken to select the separation point from the skin coefficient data, using 8C as an exemplar case. The separation point is defined where skin friction approaches zero, which for the case shown at the second corner. Streamwise position is shown with major geometric points highlighted. The red stars represent the mean skin friction coefficient for individual locations on top and bottom walls of the polygon's surface.

https://doi.org/10.59720/25-121

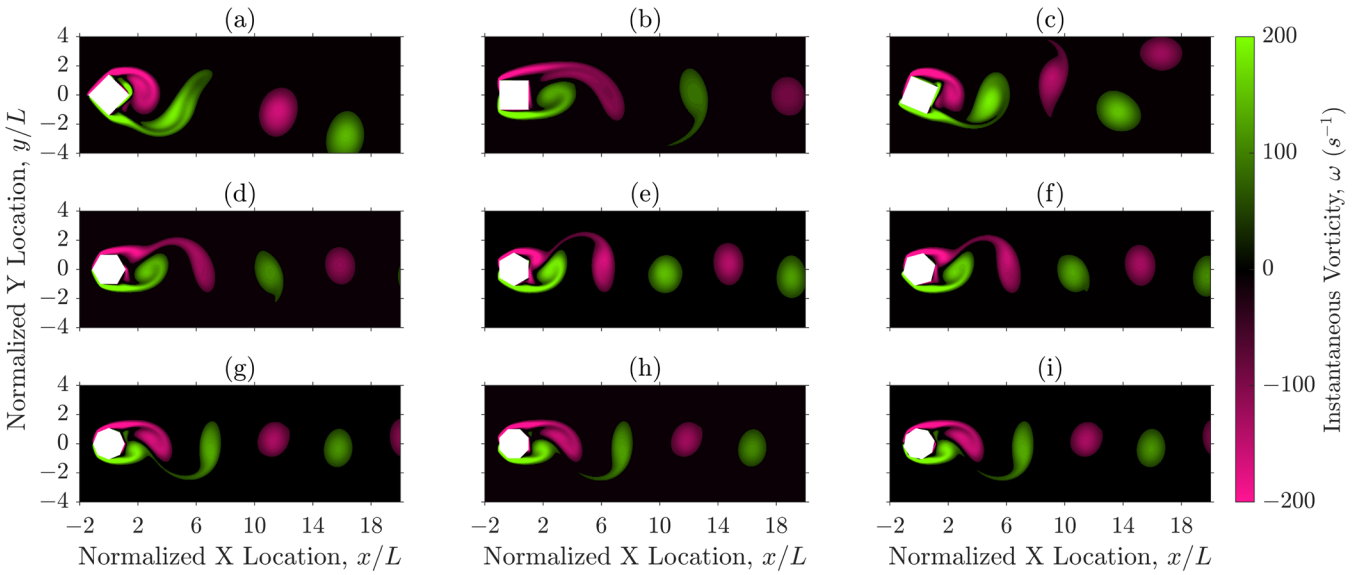

Figure 5: Contour graph of instantaneous vorticity of all test cases. A single timestep was selected and instantaneous vorticity plotted for test case 4C (a), 4F (b), 4H (c), 6C (d), 6F (e), 6H (f), 8C (g), 8F (h), and 8H (i). Green and pink regions represent counterclockwise and clockwise rotation, respectively. The axes represent the 2D spatial region around the body.

the unsteady data.

A validation study was performed to compare the model's performance in predicting unsteady loading in both magnitude and frequency. A circle was tested, with the same characteristic dimensions as the main polygons, to directly test the accuracy of the solver against prior numerical data (14). A Strouhal number of 0.19628 was obtained, and Rajani *et al.* obtained a Strouhal number of 0.1957, which is a 0.296% difference (14). While the result from this showed good prediction of numerically observed trends, the data within this work should be treated as comparative rather than absolute. Experimental conditions were kept constant throughout the experiment. To keep the characteristic length at 0.01 m, a formula was derived for the side length given the characteristic length:

$$L = 4A/p \quad \text{[Equation 1]}$$
$$A = 0.25ns^2\cot(\pi/n) \quad \text{[Equation 2]}$$
$$p = ns \quad \text{[Equation 3]}$$
$$L = s\cot(\pi/n) \quad \text{[Equation 4]}$$
$$s = L\tan(\pi/n) \quad \text{[Equation 5]}$$

where L is the characteristic length, A is the area, n is the number of sides, and s is the side length. The characteristic length is the reference length used for calculations, while the side length is a geometric length of a polygon's edge. Transient time was used to obtain a periodic lift coefficient graph, which was used to calculate the shedding period and Strouhal number.

Test cases

Nine test cases were examined by varying two parameters: side number (N = 4, 6, 8) and angular position. Three modes of rotation were defined as: face perpendicular to the fluid flow (F), corner perpendicular to the fluid flow (C), and halfway between positions F and C (H) (**Figure 3**). These cases were selected to clearly illustrate variations in Strouhal number, which relates the frequency of vortex shedding to the characteristic length and flow velocity. Commonly used in fluid dynamics to describe unsteady flow phenomena, the Strouhal number was used because it provides a direct measure of vortex shedding behavior. Prior studies have shown that polygons with more than eight sides exhibit minimal variation (7). Odd-sided shapes (e.g. N = 5) follow fundamentally different trends than even-sided shapes, so these were excluded from this study.

Simulations were run for all nine test cases, producing unsteady lift and drag outputs. A shedding frequency was derived, f, from the periodic time series of the lift, and then used to calculate the Strouhal number, $St = fL/v$, which is also dimensionless, allowing our results to be directly compared to those that would exist on different scaled structures. Other flow variables were collected, such as skin friction and vorticity, after the simulation ran to enable deeper analysis of the flowfield for each case.

Defining the separation point

For each case, the separation point was obtained by plotting the time-averaged skin friction coefficient against the position along the polygon's surface and locating the point on the polygon where $C_F \approx 0$ (**Figure 4**). The position at which the skin friction coefficient goes to zero is then converted as a percentage of the amount of characteristic length it has travelled and then turned into the corresponding angle.

Received: May 27, 2025
Accepted: November 30, 2025
Published: June 29, 2026

REFERENCES

1. Tang, Tao, *et al.* "Flow-Induced Rotation Modes and Wake Characteristics of a Circular Cylinder Attached with a Splitter Plate at Low Reynolds Numbers." *Ocean*

https://doi.org/10.59720/25-121

Engineering, vol. 266, 17 Oct. 2022, p. 112823, https://doi.org/10.1016/j.oceaneng.2022.112823.
2. Farsad, Saeed, *et al*. "Experimental Study of Vortex Shedding Phenomenon Induced by Various Bluff Body Geometries for Use in Vortex Flowmeters and Flow Angle Sensors." *European Journal of Mechanics - B/ Fluids*, vol. 111, 17 Jan. 2025, https://doi.org/10.1016/j.euromechflu.2025.01.007.
3. "Earth from Orbit: Von Kármán Vortices." *National Environmental Satellite, Data, and Information Service*, 13 May 2021, www.nesdis.noaa.gov/news/earth-orbit-von-karman-vortices. Accessed 21 May 2025.
4. Harvey, Sam Tucker, *et al*. "An Inertial Mechanism behind Dynamic Station Holding by Fish Swinging in a Vortex Street." *Scientific Reports*, vol. 12, no. 1, July 2022, https://doi.org/10.1038/s41598-022-16181-8.
5. Emanuel, Kerry A. "Some Aspects of Hurricane Inner-Core Dynamics and Energetics." *Journal of the Atmospheric Sciences*, vol. 54, no. 8, Apr. 1997, pp. 1014–26, https://doi.org/10.1175/1520-0469(1997)054%3C1014:SAOHIC%3E2.0.CO;2.
6. Ge, Yaojun, *et al*. "Case Study of Vortex-Induced Vibration and Mitigation Mechanism for a Long-Span Suspension Bridge." *Journal of Wind Engineering and Industrial Aerodynamics*, vol. 220, Jan. 2022, p. 104866, https://doi.org/10.1016/j.jweia.2021.104866.
7. Xu, S. J., *et al*. "Experimental Study of Flow around Polygonal Cylinders." *Journal of Fluid Mechanics*, vol. 812, Dec. 2016, pp. 251–78, https://doi.org/10.1017/jfm.2016.801.
8. Geyer, Thomas F. "Experimental Evaluation of Cylinder Vortex Shedding Noise Reduction Using Porous Material." *Experiments in Fluids*, vol. 61, no. 7, June 2020, https://doi.org/10.1007/s00348-020-02972-0.
9. Uzun, Dogancan, *et al*. "Does the Barnacle Settlement Pattern Affect Ship Resistance and Powering?" *Applied Ocean Research*, vol. 95, Feb. 2020, p. 102020, https://doi.org/10.1016/j.apor.2019.102020.
10. Yilin Liuhan, and Toby Bryce-Smith. "Computational Study of Erosion Effects on a Triangular Aerofoil's Aerodynamics at Reynolds Number of 10,000." *Journal of Emerging Investigators*, vol. 8, Jan. 2025, https://doi.org/10.59720/24-260.
11. "Ansys® Student 2024 R2, Free Student Software Downloads." Ansys Inc. https://ansys.com/academic/students. Accessed 21 May 2025
12. Bruce Roy Munson, *et al*. *Fundamentals of Fluid Mechanics*. 7th ed., 1999, p. 49.
13. Versteeg, H. K., and W. Malalasekera. *An Introduction to Computational Fluid Dynamics: The Finite Volume Method.* 1995.
14. Rajani, B. N., *et al*. "Numerical Simulation of Laminar Flow Past a Circular Cylinder." *Applied Mathematical Modelling*, vol. 33, no. 3, Mar. 2009, pp. 1228–47, https://doi.org/10.1016/j.apm.2008.01.017.